Theoretical Understanding of the Interprotein Electron Transfer between Cytochrome c_2 and the Photosynthetic Reaction Center

Osamu Miyashita, Melvin Y. Okamura, and José N. Onuchic*

Center for Theoretical Biological Physics and Department of Physics, University of California at San Diego, 9500 Gilman Drive, La Jolla, California 92093-0319

Received: August 13, 2002; In Final Form: November 14, 2002

Interprotein electron transfer (ET) reactions play a central role in the early steps in bioenergetic processes such as photosynthesis and respiration. This paper describes initial advances in the theoretical understanding of the interprotein electron transfer between cytochrome c_2 and the photosynthetic reaction center in *Rhodobacter sphaeroides* from calculations based on the recently determined X-ray crystal structure.[1] Dynamical effects at the protein−protein interface of the docked complex, which mediates the ET, are investigated by calculating the protein and solvent (low-frequency) contributions to the reorganization energy. Since this interface contains almost no solvent, the low-frequency contributions to the reorganization energy are small (a few tenths of an electronvolt). The small value of the reorganization energy is consistent with experimental results if high-frequency (quantum) modes due to cofactor vibrations are taken into account. The results indicate that the mutational effects on the Franck−Condon factor are likely to be small. Influences on the tunneling matrix element have also been investigated. Utilizing an approach that integrates molecular dynamics and the Pathways method, we have observed that the ensemble dominant tunneling pathways in this reaction go though the tyrosine L162 and can be water mediated.

1. Introduction

Electron-transfer reactions are one of the most fundamental processes in biological systems, affecting processes such as photosynthesis, oxidative phosphorylation, drug metabolism, DNA damage, and many enzymatic reactions. In searching for a more quantitative understanding of these reactions, the past decade has seen tremendous growth in the development of reliable molecular-level theories and models for intramolecular biological electron transfer (ET) reactions (for reviews, see refs 2−5). Among these processes, the mechanism of electron transfer in photosynthesis is of great interest (for reviews, see refs 6 and 7). In the photosynthetic reaction center, the optical excitation of the special pair of bacteriochlorophyll $(BChl)_2$ triggers charge-separation reactions that consists of intramolecular ET steps between pigments in the reaction center.

By utilizing these new theoretical approaches with the aid of several new relevant protein structures, it is now possible to start to explore fully entire bioenergetic processes such as photosynthesis and respiration. Some of the interesting steps in these processes involve interprotein ET reactions, which is a topic that has received limited theoretical attention until now. In these systems, water-soluble ET proteins such as *c*-type cytochromes shuttle electrons between specific electron donor and acceptor protein complexes in membranes. Compared to intraprotein reactions, the mechanism of interprotein ET reactions has increased in complexity since these reactions include an additional association process of the different proteins that house the donor and acceptor sites. In addition, even the unimolecular ET step after the protein complex is formed may have different character compared to that of the intraprotein reactions. The transferring electron has to go through the protein−protein interface, which may be much more flexible than the protein core that solely comprises the tunneling medium for the intraprotein case. Water molecules may also profoundly affect this interface.

The system studied in this paper is the interprotein ET reaction involved in the reduction process of the photosynthetic reaction center (RC) by the electron shuttle protein, cytochrome c_2 (cyt c_2). Cyt c_2 transports electrons from cyt bc_1 to the oxidized primary donor in the RC. Extensive experimental studies have been performed to understand this ET reaction between cyt c_2 and the RC in bacterium *Rhodobacter sphaeroides*. A key question is how this reaction rate is controlled by the protein environment. Recently, the X-ray structure of a cocrystal of the cyt c_2/RC complex has been obtained by Axelrod et al.[1] This new structural information enables us to start numerical simulations and theoretical studies of this interprotein ET rate in the protein complex.

In this paper, we describe a series of new theoretical advances needed to explore these more challenging ET reactions theoretically by generalizing our earlier approaches for intraprotein reactions. Typically, long-distance ET reactions, which are mediated by the protein environment, have an electronic coupling between the donor and acceptor sites that is sufficiently weak that the rate calculation can be made at the nonadiabatic limit. In this nonadiabatic regime, the reaction is controlled by two main factors: a nuclear factor that determines the thermally averaged density of states in which the reactant (transfer electron in the donor) and product (transfer electron in the acceptor) electronic states are resonant and therefore electron tunneling between them is possible. These resonant configurations are called the activated complex. The second factor is the electronic coupling between donor and acceptor states that determines the tunneling frequency between them. The reaction rate is a product of these two factors and can be written by utilizing Fermi's Golden Rule:[8−10]

* Corresponding author. E-mail: jonuchic@ucsd.edu.

10.1021/jp026753k CCC: $25.00
Published on Web 01/10/2003

$$k_{ET} = \frac{2\pi}{\hbar}|T_{DA}|^2 \,(FC) \quad (1)$$

where $\hbar$ is Planck's constant divided by 2π, T_{DA} is the electronic tunneling matrix element for the electron donor (D)−acceptor (A) pair, and FC is the Franck−Condon factor associated with the nuclear thermal activation.

1.1. Protein Control of the Franck−Condon Factor: Quantum and Classical Contributions. As discussed above, the FC factor is the thermally averaged (over the reactant state) density of states at the nuclear configuration(s) in which the donor (reactant) and acceptor (product) electronic states are resonant. Protein and solvent fluctuations provide fluctuations of the electric field felt by the donor and acceptor states and therefore modulate their energy.

These nuclear motions are commonly divided into two classes of modes. The first class consists of mostly local modes (close to the donor and acceptor sites), with frequencies sufficiently high that they have to be treated in the quantum regime; these modes are typically inner-sphere contributions to the reorganization energy. The second one contains modes that are much more delocalized over the protein environment and solvent. These are low-frequency motions that can be treated in the classical limit and are studied in this paper with the aid of classical molecular dynamics simulations.

As we have discussed, the system of interest in this work is the ET reaction between the heme group in cyt c_2 and the special pair in the RC. In particular, we focus on the contributions from the interface region between cyt c_2 and the RC that are experimentally varied by protein engineering. A possible source for the FC quantum contribution may come from hydrogen bond fluctuations in the region of the special pair that is coupled to the ET reaction.[11−13] Several theoretical studies[14−21] have provided the tools to understand these high-frequency modes. Regarding the low-frequency motions, the classical contribution to the reaction free energy and the reorganization energy of the ET reaction or the charge insertion processes have been studied by several groups.[22−31] In this paper, although we do not directly compute the quantum contribution, we are able to separate (in section 4.1) the classical contribution from the experimentally determined FC factor.[32] Assuming that the contributions from high- and low-frequency modes are important, the classical reorganization energy is around 300 meV (see section 4.1 for a more careful analysis). This small value for the classical reorganization energy is expected since in the bound state both the donor and acceptor sites are sufficiently isolated from the solvent.

1.2. Protein Control of the Tunneling Matrix Element. The dynamical properties of protein and solvent molecules are also important for the tunneling matrix elements. Recently, the effect of conformational fluctuation on the tunneling matrix element has been studied.[33,34] These results showed that the tunneling matrix element calculated for the X-ray structure is not necessarily representative of its average contribution during the thermal fluctuation of the system. The flexibility of protein molecules is very important in modulating this coupling.

Recent theoretical developments for computing donor−acceptor interactions or tunneling matrix elements provide the tools needed for determining how the protein structure mediates this coupling. These methods include empirical (Pathways[35,36] and protein packing density analysis[37]) and semiempirical electronic structure methods (extended Hückel[38−43] and neglect of differential overlap methods[44,45]) and ab initio divide-and-conquer methods.[46] Many examples exist where theoretical analysis has led to specific testable predictions[47] and to the design of key mutagenesis experiments or has helped to explain otherwise puzzling experimental results.[48−51]

In this paper, we extend our study to the interprotein ET reaction from cyt c_2 to RC. We perform a classical molecular dynamics simulation that samples the conformational space around the co-crystal structure. In the bound structure, solvent molecules are allowed to move in and out of the protein−protein interface. Our analysis is able to explain several of the recent experiment observations. For example, measurements of the first-order ET rates show that they are weakly dependent on mutations.[52] Other experimental data of *Rhodopseudomonas viridis* also show the same tendency even for mutation Tyr162 of the RC L unit, which is located midway between redox sites.[53] To understand these results, the importance of each residue to the reaction is discussed from the analysis of simulation.

2. Theoretical Tools to Analyze Simulation Data: The Classical FC Factor and Electronic Coupling

In this section, we describe the theoretical models utilized to analyze the simulation data. Section 2.1 reviews the general theory for the Franck−Condon (FC) factor, especially the different contributions from the inner-sphere (high-frequency modes) and classical outer-sphere (delocalized modes) reorganization energy. In Section 2.2, we describe how this classical component can be obtained from our simulations. In Section 2.3, strategies to partition the reorganization energy contribution from different physical regions of the protein/solvent are discussed. This is particularly needed to analyze the contributions from the protein−protein interface region. Finally, Section 2.4 describes the Pathways model, which is used to evaluate how the tunneling matrix element varies during the dynamical trajectories.

2.1. Franck−Condon Factor. When electron transfer takes place between the donor and acceptor sites, the energy associated with the reaction driving force ($-\Delta G$) is dissipated into the high- and low-frequency modes as described above. In the nonadiabatic limit, the general rate expression, which separates these two contributions, can be written as[16,21]

$$k = \sum_{hf}\frac{2\pi}{\hbar}T_{DA}^2[FC^{hf}(E_{hf})]\frac{1}{\sqrt{4\pi k_B T\lambda_c}} \times \exp\left[-\frac{(\Delta G + E_{hf} + \lambda_c)^2}{4k_B T\lambda_c}\right] \quad (2)$$

where FC^{hf} is the contribution to the FC factor by the high-frequency modes and E_{hf} is the energy dissipated by them. The energy dissipated by the low-frequency modes is therefore $-\Delta G - E_{hf}$. λ_c is the reorganization energy from the slow modes (i.e., the classical contribution). For small driving forces (smaller than a high-frequency mode "vibron"), no energy can be damped into the high-frequency modes, and the driving-force energy is totally dissipated into the low-frequency part of the FC. In this regime, because $E_{hf} = 0$,[17] only the first term in the sum of eq 2 has to be considered. Therefore, the temperature dependence of the rate is fully determined by the classical part of the FC factor and is given by Marcus relation,[8]

$$FC = \frac{1}{\sqrt{4\pi k_B T\lambda_c}}\exp\left[-\frac{(\Delta G + \lambda_c)^2}{4k_B T\lambda_c}\right] \quad (3)$$

This result will be particularly important in section 4 when we

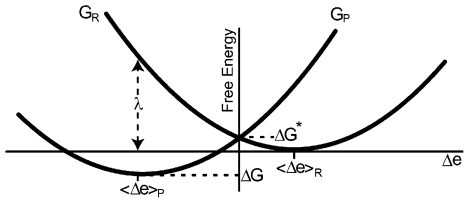

Figure 1. Schematic representation of the free-energy profiles of the product, G_P, and the reactant status, G_R. The free energy is defined by the reaction coordinate, Δe, which is the energy gap between the reactant and the product states. The reaction free energy, ΔG, is defined as the free energy of the product state minus that of reactant state, thus $(-\Delta G)$ corresponds to the driving force. Note that Δe is not a spatial coordinate.

separate the low-frequency contribution from the total reorganization energy from the experimentally measured rates.

2.2. Determining the Classical FC Factor from Simulations. The classical reorganization energy λ_c is determined from simulations utilizing the following theoretical procedure (see ref 5 for more details). The subscript c is now dropped from the reorganization energy since we refer only to the classical reorganization energy in the remainder of section 2. In the limit where Marcus theory is valid, we can describe the low-frequency reaction coordinate as being a quadratic function of a single global reaction coordinate, q, with different equilibrium positions for the reactant ($U_R(q)$) and product ($U_P(q)$) surfaces. If that is the case, this global reaction coordinate, q, will be linearly related to the energy gap ($\Delta e = (U_R(q) - U_P(q))$ between the reactant and product surfaces, and the probability distribution of this energy gap should be Gaussian with a width that linearly increases as the temperature is raised.

Since there is this linear dependence between the energy gap and any appropriate choice of the global reaction coordinate, it is a convenient choice[54] to use this gap Δe as the reaction coordinate in our simulations. By verifying that its probability distribution is Gaussian, we can determine if Marcus theory is appropriate. Electron transfer occurs at the resonant states (i.e., $U_R = U_P$ ($\Delta e = 0$)), and the classical FC factor is the thermally averaged reactant density of state at $\Delta e = 0$. With Δe as the reaction coordinate, the free-energy profiles for the reactant and product surfaces, $G_R(\Delta e)$ and $G_P(\Delta e)$, respectively, are defined as

$$G_R(\Delta e) = -\frac{1}{\beta}\log\int \mathrm{d}q\, e^{-\beta U_R(q)}\delta(\Delta e - \Delta e(q)) \quad (4)$$

$$G_P(\Delta e) = -\frac{1}{\beta}\log\int \mathrm{d}q\, e^{-\beta U_P(q)}\delta(\Delta e - \Delta e(q)) \quad (5)$$

where $\beta = 1/k_B T$. From these definitions, an exact relation can be derived:[18,54-56]

$$G_P(\Delta e) - G_R(\Delta e) = \Delta e \quad (6)$$

Thus, if the free energy of the system has a quadratic dependence on Δe, then $G_R(\Delta e)$ and $G_P(\Delta e)$ must be parabolas with the same curvature. They can be characterized by the two parameters λ and ΔG (see Figure 1); the former, λ, is the reorganization energy, and the latter, ΔG, is the reaction free energy,

$$G_R(\Delta e) = \frac{1}{4\lambda}(\Delta e - \Delta G - \lambda)^2 \quad (7)$$

$$G_P(\Delta e) = \frac{1}{4\lambda}(\Delta e - \Delta G + \lambda)^2 + \Delta G \quad (8)$$

As can be seen in eqs 7 and 8, the reorganization energy, λ, is related to the curvature of the parabola. From this fact, λ is related to the magnitude of fluctuation of the reaction coordinate in equilibrium as[27]

$$\lambda = \frac{1}{2}\beta\langle \Delta e^2\rangle_c \quad (9)$$

where $\langle\ \rangle_c$ indicates the cumulant average.[57] Note that this average does not depend on whether averaging is on the reactant or product surface. However, from the relations $\langle\Delta e\rangle_R = \Delta G + \lambda$ and $\langle\Delta e\rangle_P = \Delta G - \lambda$, which can be derived from eqs 7 and 8, the reorganization energy can be defined as

$$\lambda = \frac{1}{2}(\langle\Delta e\rangle_R - \langle\Delta e\rangle_P) \quad (10)$$

where $\langle\ \rangle_R$ and $\langle\ \rangle_P$ indicate the averages of the reactant and product states, respectively. This definition was used in a linear response approximation, LRA, approach.[58-60]

2.3. Component Analysis of the Reorganization Energy. An additional benefit from the simulation studies is the ability to obtain microscopic information. Molecular dynamics simulation enables us to understand the total reorganization energy as the sum of contributions that originate from different parts of the protein complex. The electron-transfer reaction system consists of three parts—donor, acceptor, and the environment that comprise the proteins and the water molecules. During ET, the charges on the atoms in the redox sites vary. Thus, the energy difference $\Delta e = U_P - U_R$ is a consequence of the change in the electrostatic interactions between the redox sites and the environment. Formally, we can write $\Delta e \propto \Delta q q'/r$, where Δq is the change in the charge of the redox site, q' is the charge of the environment, and r is the distance between them. This Δe can now be partitioned into any desired components. For example, we can divide this value into contributions from the donor (D) and the acceptor (A), $\Delta e \propto \Delta q_A q'/r + \Delta q_D q'/r$. In addition, they can be divided into contributions from the protein (P) and the water (W) molecules as $\Delta e \propto \Delta q_A q'_P/r + \Delta q_D q'_P/r + \Delta q_A q'_W/r + \Delta q_D q'_W/r$.

In this way, the energy difference Δe can be divided into any choice of components. The reorganization energy, however, cannot be divided in such a simple way. To discuss the division of reorganization energy into different contributions, we consider the situation where the total energy difference is divided two parts, $\Delta e = \Delta e_1 + \Delta e_2$. From the definition of eq 9, we write[25,27]

$$\begin{aligned}\lambda &= \frac{\beta}{2}\left\langle \left(\Delta e_1 + \Delta e_2\right)^2\right\rangle_c \\ &= \underbrace{\frac{\beta}{2}\left\langle \Delta e_1^2\right\rangle_c}_{\lambda_{11}} + \underbrace{\frac{\beta}{2}\left\langle \Delta e_1 \Delta e_2\right\rangle_c}_{\lambda_{12}} + \underbrace{\frac{\beta}{2}\left\langle \Delta e_2 \Delta e_1\right\rangle_c}_{\lambda_{21}} + \underbrace{\frac{\beta}{2}\left\langle \Delta e_2^2\right\rangle_c}_{\lambda_{22}}\end{aligned} \quad (11)$$

This way of partitioning was used for the studies of cyt *c*.[25,27] The above definition includes two kinds of terms. The first kind is the variance of a component of Δe such as λ_{11}. The second type is the covariance of two components of Δe such as λ_{12}. Thus, the total reorganization energy is given as a sum of variances and covariances of these component terms. Note that two covariance terms are identical from the definition (i.e., $\lambda_{12} = \lambda_{21}$). In the following discussion, we use a variance−covariance matrix representation as a way to decompose the total reorganization energy. The diagonal terms of the matrix correspond to variance terms or the fluctuation of the each component of Δe. The off-diagonal terms correspond to covariance terms, which represent the correlation between the two components of Δe. Note that the variance−covariance

matrix is a symmetric matrix. The existence of off-diagonal terms makes it difficult to decompose the total reorganization energy into several components. We call this definition the matrix definition.

However, from the definition of eq 10, the reorganization energy can be divided as[22]

$$\begin{aligned}\lambda &= \frac{1}{2}\left(\langle \Delta e_1 + \Delta e_2\rangle_R - \langle \Delta e_1 + \Delta e_2\rangle_P\right) \\ &= \underbrace{\frac{1}{2}\left(\langle \Delta e_1\rangle_R - \langle \Delta e_1\rangle_P\right)}_{\lambda_1} + \underbrace{\frac{1}{2}\left(\langle \Delta e_2\rangle_R - \langle \Delta e_2\rangle_P\right)}_{\lambda_2}\end{aligned} \tag{12}$$

With this definition, the total reorganization energy can apparently be divided into component terms. This definition was used for the studies of the reorganization energy of cyt *c*.[22] In this paper, it is called the LRA definition.

We now compare these two definitions—the matrix definition, eq 11, and the LRA definition, eq 12. For any quantity $A(q)$, the following average can be defined

$$\begin{aligned}\langle A\rangle_P &= \int dq\, e^{-\beta U_P} A / \int dq\, e^{-\beta U_P} \\ &= \int dq\, e^{-\beta U_R} e^{-\beta \Delta e} A / \int dq\, e^{-\beta U_R} e^{-\beta \Delta e} \\ &= \langle e^{-\beta \Delta e} A\rangle_R / \langle e^{-\beta \Delta e}\rangle_R\end{aligned} \tag{13}$$

Thus, $2\lambda_1$ of eq 12 can be changed as follows

$$\begin{aligned}\langle \Delta e_1\rangle_P - \langle \Delta e_1\rangle_R &= \langle \Delta e_1 - \langle \Delta e_1\rangle_R\rangle_P \\ &= \langle e^{-\beta \Delta e}(\Delta e_1 - \langle \Delta e_1\rangle_R)\rangle_R / \langle e^{-\beta \Delta e}\rangle_R\end{aligned} \tag{14}$$

by the cumulant-expansion theorem,[57] and if we assume that the third and higher cumulant averages are negligible,

$$\log\langle e^{-\beta \Delta e}\rangle_R = \langle e^{-\beta \Delta e} - 1\rangle_{c,R} = \left\langle -\beta \Delta e + \frac{\beta^2}{2}\Delta e^2\right\rangle_{c,R} \tag{15}$$

then,

$$\begin{aligned}\langle \Delta e_1\rangle_P - \langle \Delta e_1\rangle_R = \\ \langle e^{-\beta \Delta e}(\Delta e_1 - \langle \Delta e_1\rangle_R)\rangle_R / \exp\left(\left\langle -\beta \Delta e + \frac{\beta^2}{2}\Delta e^2\right\rangle_{c,R}\right) \\ = \langle e^{-\beta \delta \Delta e}\, \delta \Delta e_1\rangle_R / \exp\left(\left\langle \frac{\beta^2}{2}\delta \Delta e^2\right\rangle_{c,R}\right)\end{aligned} \tag{16}$$

where $\delta \Delta e_1 = \Delta e_1 - \langle \Delta e_1\rangle_R$. For the variables x_1 and x_2, whose averages are zero and their third- and higher-order fluctuations are zero, by the cumulant-expansion theorem,

$$\langle e^{b_1 x_1 + b_2 x_2}\rangle = \exp(\langle (b_1 x_1 + b_2 x_2)^2\rangle) \tag{17}$$

and the partial derivative relative to b_1 gives

$$\langle x_1 e^{b_1 x_1 + b_2 x_2}\rangle = 2\langle x_1 (b_1 x_1 + b_2 x_2)\rangle \exp(\langle (b_1 x_1 + b_2 x_2)^2\rangle) \tag{18}$$

By setting $b_1 = b_2 = -\beta$, we obtain

$$\langle x_1 e^{-\beta(x_1 + x_2)}\rangle = -2\beta \langle x_1 (x_1 + x_2)\rangle \exp(\beta^2 \langle (x_1 + x_2)^2\rangle) \tag{19}$$

Finally,

$$\langle \Delta e_1\rangle_P - \langle \Delta e_1\rangle_R = -\beta \langle \delta \Delta e_1 \delta \Delta e\rangle_R \tag{20}$$

From the result above, we conclude that the contribution λ_1 in eq 12 is equal to $\lambda_{11} + \lambda_{12}$ in eq 11. Generalizing, these two definitions are related as

$$\lambda_i = \sum_j^n \lambda_{ij} \tag{21}$$

where n is the number of elements of decomposition. Thus, it is also true that sums of columns or rows of the variance−covariance matrix from definition of eq 11 give the corresponding component of eq 12. This situation is similar to the discussions regarding the component of the free-energy calculation.[61] The expression for the reaction free energy (i.e., driving force) can be

$$\Delta G = -\frac{1}{\beta}\ln\langle \exp[-\beta \sum_k \Delta e_k]\rangle_R \tag{22}$$

With the cumulant-expansion theorem, this equation can also be expanded as

$$\begin{aligned}\Delta G &= \langle \Delta e\rangle_R - \frac{\beta}{2}\langle \Delta e^2\rangle_{R,c} + \cdots \\ &= \langle \Delta e_1\rangle_R + \langle \Delta e_2\rangle_R - \frac{\beta}{2}\langle \Delta e_1{}^2\rangle_{R,c} - \frac{\beta}{2}\langle \Delta e_2{}^2\rangle_{R,c} - \\ &\qquad \beta \langle \Delta e_1 \Delta e_2\rangle_{R,c} + \cdots\end{aligned} \tag{23}$$

The reorganization energy is identical to the term $O(\beta)$, and the correlation term is included. However, we can define the free-energy component with the thermodynamic integration equation of the linear path[62,63] as

$$\begin{aligned}\Delta G = \Delta G_1 + \Delta G_2 + \cdots = \\ \int_0^1 dk\, \langle \Delta e_1\rangle_k + \int_0^1 dk\, \langle \Delta e_2\rangle_k + \cdots\end{aligned} \tag{24}$$

where the average over k indicates the averaging under the potential of $(1 - k)U_R + kU_P$. Each free-energy component can be expanded as[61]

$$\Delta G_1 = \langle \Delta e_1\rangle_R - \frac{\beta}{2}\langle \Delta e_1{}^2\rangle_{R,c} - \frac{\beta}{2}\langle \Delta e_1 \Delta e_2\rangle_{R,c} \tag{25}$$

$$\Delta G_2 = \langle \Delta e_2\rangle_R - \frac{\beta}{2}\langle \Delta e_2{}^2\rangle_{R,c} - \frac{\beta}{2}\langle \Delta e_1 \Delta e_2\rangle_{R,c} \tag{26}$$

The second term, which corresponds to the reorganization energy, is partitioned symmetrically between ΔG_1 and ΔG_2, which is the same situation as for the decomposition of the reorganization energy with eq 12.

The benefit of the LRA definition used in eq 12 is that the component terms are additive (i.e., the sum of the components λ_i's is equal to the total reorganization energy). We cannot ignore, however, that each of these components also includes a correlation contribution. Correlation effects have shown to be strong[25,27] since in most cases the reorganization energy has contributions from interactions of different regions. In this sense, the variance−covariance matrix representation is more appropriated to partition the total reorganization energy. In the analysis of molecular dynamics simulation, we use the matrix representation as the original information. A comparison between these two approaches is also presented.

2.4. Pathways Model for Tunneling Matrix Element Calculations. The electronic tunneling matrix element, T_{DA}, of eq 1 is related to the strength of the electronic interaction between the donor and acceptor. Utilizing the tunneling Pathways model[64−66] of Beratan and Onuchic, we explore the

effects of dynamical fluctuations on the tunneling coupling. The Pathways model assumes that a pathway tube controls the coupling between the donor and acceptor and therefore determines an algorithm to identify this dominant tube. The numerical implementation of this method assigns a "decay" factor for the different kinds of orbital contacts in a protein. An electron tunneling pathway is defined as a product of these decays via covalent (C), hydrogen-bonded (H), or through-space (S) connections. For a single pathway, the coupling is approximated as[64−66]

$$T_{DA} \propto \prod_i \epsilon_i^C \prod_j \epsilon_j^S \prod_k \epsilon_k^H \tag{27}$$

As a simple implementation of the Pathway model, we chose the following parameters:[35,67]

$$\epsilon^C = 0.6 \tag{28}$$

$$\epsilon^H = (0.6)^2 \exp[-1.7(R - 2.8)] \tag{29}$$

$$\epsilon^S = 0.6 \exp[-1.7(R - 1.4)] \tag{30}$$

The distances between heavy atoms, R, are in angstroms, and the decay factors, ϵ, are unitless. These relationships have been successful in predicting the electronic coupling in several ET proteins such as azurin and cyt *c*.[35,67]

In our pathway calculations, hydrogen bond couplings are distance-scaled as in a standard model.[35,67] An alternative model[48,68] of these distance fluctuations treats the hydrogen bonds as two covalent bonds (i.e., $\epsilon_H = \epsilon_C^2$). We have used the original definition because the hydrogen bonds at the interface between the proteins are likely to exhibit a larger range of distances than hydrogen bonds in the protein core. In this interface, hydrogen bonds are made and broken between water molecules and the protein surfaces and therefore are much less constrained than they are inside the protein.

3. Simulation Methods

Utilizing the theoretical framework described above, we studied the electron-transfer reaction from cyt c_2 to RC. To obtain information about the thermal fluctuations of the system, we performed molecular dynamics simulations. The simulated trajectory was analyzed with the methods described in section 2. Section 3.1 describes the procedure utilized for the molecular dynamics simulation. Section 3.2 describes how these simulation results were used for the calculation of reorganization energy and in section 3.3 for the calculation of tunneling matrix elements.

3.1. Molecular Dynamics Simulation. We have carried out molecular dynamics simulations of the cyt c_2/RC from *Rb. sphaeroides*. For the simulations, the protein coordinates of the cyt c_2/RC complex from X-ray studies by Axelrod et al.[1] were used. To simulate the effects of the solvent on ET between two redox sites, water molecules were placed to fill a sphere with a 30-Å radius centered on the iron of the heme. Explicit water molecules (1730) were included. No counterion was included. Since the H unit of RC is far from the redox sites, it was removed to reduce the size of the system to be simulated. Thus, 17 022 atoms were included in the simulation. Figure 2 shows the structure of the complex prior to simulations. We used the partial charges published previously for the reduced heme group.[70] For the oxidized heme group, we used the charges reported in a previous study of cytochrome *c*,[25,71] which was prepared by using a charge distribution of reduced and oxidized

Figure 2. Schematic representation of the prepared structure for the "solvated" complex of cytochrome (cyt) c_2 and the photosynthetic reaction center (RC) utilized in our calculations. The X-ray co-crystal structure bound state of cyt c_2 and the RC was used as the initial coordinate of the molecular dynamics simulation. The system was solvated so that water molecules filled a sphere of 30-Å radius centered on the iron of the heme. The H unit is not included in the simulation. The Figure was made with Molscript.[76]

porphines.[72] The partial charges of the reduced and oxidized bacteriochlorophyll, bacteriopheophytin, and ubiquinone RC cofactors were obtained by restricted and unrestricted Hartree−Fock calculations with the PM3 basis set using the GAMESS package.[73] Additional parameters for these compounds are taken from the AMBER parameter set.[74] The standard AMBER94 force field[74] was used for the protein atoms, and the TIP3P model was used for water molecules.[75] All ionizable side chains were configured in their characteristic ionized states at pH 7.0, and all nonliganding histidines were treated as neutral with a proton on ND1.

The AMBER6 program package[77] was used to carry out the molecular dynamics simulations. Long-range electrostatic and VDW interactions were treated with a 20-Å cutoff. For the calculations of electrostatic interactions, we performed three calculations with a dielectric constant of $\epsilon = 1$, 2, or 4. CAP boundary potentials were used to constrain the position of the water molecules near the protein. Weak constraints (10^{-2} kcal mol^{-1} Å^{-2}) were imposed on the main chain atoms to keep shape of RC and to prevent the dissociation of the cyt c_2 from the RC. It is weak enough to provide some flexibility to the main chain. The positions of the side-chain atoms were not constrained, which is fundamental to have the appropriate dynamics at the protein−protein interface.

Energy minimization was performed for the coordinates with a suitable combination of the steepest descent and conjugate gradient techniques. Following the energy minimization step, molecular dynamics simulations were carried out to equilibrate the system at 300 K. Finally, a 1-ns simulation run was performed to generate the ensemble of structures used in this study. The minimization and the molecular dynamics simulation were performed with the heme on cyt c_2 in the reduced state (cyt c_2^{2+}) and the $(BChl)_2$ on the RC in the photooxidized radical cation state $(BChl)_2^{+\bullet}$. Thus, the reaction investigated is cyt c_2^{2+}/$RC^+ \rightarrow$ cyt c_2^{3+}/RC.

3.2. Calculation of Reorganization Energy. The calculation of the classical reorganization energy utilized 10 000 structures

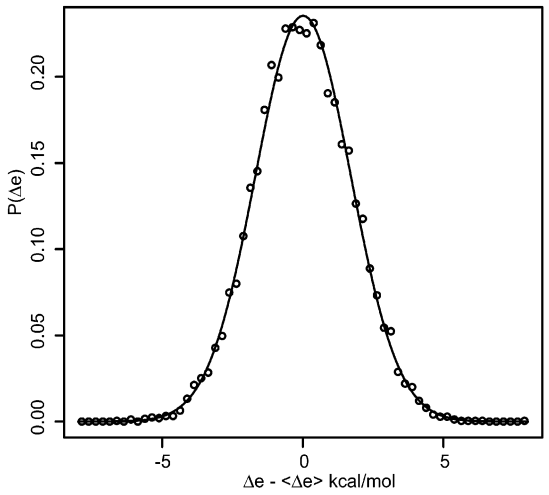

Figure 3. Probability distribution of the energy difference, Δe, during a 1-ns molecular dynamics simulation. The distribution is fitted by a Gaussian curve. The good fit indicates the harmonisity of free-energy profiles G_P and G_R, which support the framework of formulations.

obtained during the 1-ns run (i.e., 1 per 100 fs). For each structure, the electrostatic energy was calculated for both the reactant and product states to determine Δe. In the electrostatic calculation, interactions within redox sites are omitted because these energies should be included in the quantum contribution. The classical contribution has to be extracted from the experimental data before a comparison to our simulation results can be performed. This comparison is presented in section 4.1.

3.3. Calculation of Pathways Decay Factor. The modulation of the Pathways decay factor by protein thermal motions is also investigated with the aid of the 1-ns trajectory. For each transient structure stored during the simulation (1000 structures, 1 per ps), we identified the specific pathway that maximizes the heme−$(BChl)_2$ electronic coupling. A program incorporating the algorithm of Betts et al.[78] was coded in JAVA language and used for Pathways calculations. In these calculations, water molecules included in the molecular dynamics were considered to be functional components for electron tunneling.

4. Results and Discussions

In this section, we present the results of simulations obtained with the methods described above and establish a quantitative comparison to the experimental results. The effect of the protein−protein interface on both the tunneling matrix element and the classical reorganization energy can now be understood.

4.1. Comparing the Calculated and Experimentally Determined Classical Reorganization Energy. Following the procedure described in section 2.1, the classical reorganization energy was determined. Figure 3 shows the probability distribution of Δe. This probability distribution can be fitted well by a Gaussian curve, thus free-energy profiles (eq 4) are harmonic, which validates the methods described in section 2. The total reorganization energy is then calculated using eq 9. The values for this reorganization vary from 2.4 kcal/mol (∼0.10 eV) for a dielectric constant of 4 to 15 kcal/mol (∼0.64 eV) for a dielectric constant of 1 (see Table 1). In principle, if the force fields included all of the polarization effects properly, then the latter value would be correct. Since these values tend to overestimate the total reorganization energy, results are presented for corrections for different values of the dielectric constant. Although the precise value of the classical reorganization energy depends on the specific choice of the dielectric constant, the analysis presented in section 4.2, which determines the parts of the protein that dominate the reorganization energy, is independent of it. The numerical values of that section are computed for a dielectric constant of 4, but they scale similarly to the total reorganization energy (as shown in Table 1) if a different choice is taken. Thus, though the uncertainty of the values of the dielectric constant makes the quantitatively precise evaluation of the reorganization energy very difficult, these difficulties do not affect our main interest (i.e., the relative importance of various component terms).

TABLE 1: Relation between the Reorganization Energy and the Dielectric Constant

dielectric constant	reorganization energy (kcal/mol)	reorganization energy (meV)
1.0	14.80	642
2.0	6.39	277
4.0	2.41	104

We now compare this theoretical result to experiments. If all of the reorganization energy is assumed to be classical, then when analyzing their experimental data Lin et al. reported a total reorganization energy of 500 meV,[79] and succeeding studies by Venturoli et al. estimated this value to be 960 meV.[32] Venturoli et al., however, measured these rates for different temperatures (varying between 300 and 220 K) and for series of specifically mutated reaction centers characterized by altered midpoint redox potentials of P+/P varying from 410 mV to 765 mV. From this complete set of data, one observes two interesting behaviors. The ET rates become weakly dependent on temperature, and the driving force for $|\Delta G| > 300$ meV. Also, the temperature dependence for $|\Delta G| < 300$ meV appears to indicate a classical reorganization energy around 300 meV and not around 1 eV. These two facts suggest that the reorganization energy includes important contributions from both classical and quantum modes. Therefore, we analyze these data utilizing eq 2 in section 2.1 that provides the full expression for the ET rate that incorporates both of these contributions. The overall Franck−Condon factor is a sum of Gaussians with the width determined by the classical reorganization energy and the position and intensity of each Gaussian determined by ET coupling to the high-frequency quantum modes.[16] By fitting the low driving-force range of the experimentally measured rate to a single Gaussian, we can determine the classical reorganization energy. In this region, only the first Gaussian (when no energy is dissipated into the high-frequency modes) contributes to the Franck−Condon factor; therefore, it can be used to determine λ_c.

Utilizing the formalism of section 2.1, we have reexamined their experimental data by separating the classical contribution of the reorganization energy from the quantum contribution. The experimental data of Venturoli et al.[32] shown in Figure 5 shows strong ΔG and temperature dependences for small driving forces in the range of $|\Delta G| < 300$ meV (see Figure 6 in ref 16 for comparison), as expected since the Franck−Condon factor is affected by single Gaussian and is weakly dependent for larger driving forces. From this small driving-force region, we determined the classical reorganization energy. Although there are uncertainties in determining the precise maximum of the first Gaussian (in the low driving-force region) as well as in allowing or not allowing minor corrections to the driving force (the precise value of $|\Delta G|$ in the ET reaction may be slightly displaced from the value determined by combining the donor and acceptor redox potentials), a classical reorganization energy can be estimated in the range of 200−300 meV. These results are consistent with the ones determined by simulation described above. This small value for the classical reorganization energy

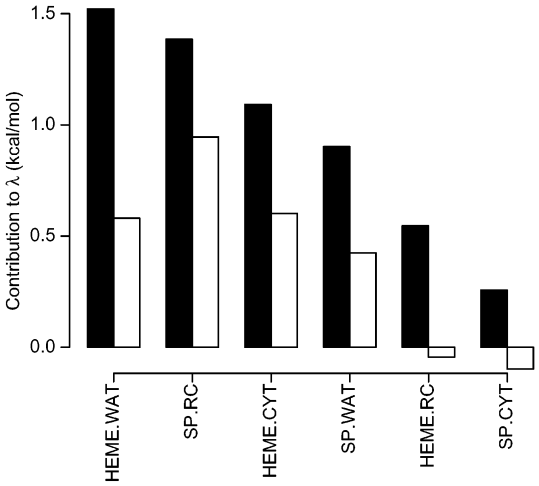

Figure 4. Contribution to the total reorganization energy from components based on the unit. HEME represents the heme moiety; SP, the special pair or $(BChl)_2$; RC, the reaction center except $(BChl)_2$; and CYT, cytochrome c_2 except the heme moiety. Thus, HEME.WAT represents the Δe coming from the interaction between the heme moiety and water molecules. The black bars represent the diagonal term variance−covariance matrix (which is Table 2), and white bars represent the sum of the row (or column) (i.e., LRA definition). The difference between them is due to the mainly negative correlations between component terms.

is expected since ET is dominated by structures around the bound complex; otherwise, tunneling would be too slow. Therefore, from this global comparison, we feel confident that our simulation quantitatively incorporates most of the energetic contributions to the classical reorganization energy, and it can be used for the more-detailed analysis that follows.

4.2. Detailed Analysis of the Classical Reorganization Energy. Contributions of Different Parts of the System. The initial analysis investigates the solvent (water) and protein contributions to the classical reorganization energy. In addition, since the system under study is an intermolecular protein ET, we investigate contributions from donor protein, cyt c_2, and acceptor proteins, RC. Therefore, this analysis is performed by dividing the system into the donor (HEME), the acceptor (SP), cyt c_2 (CYT), the photoreaction center (RC), and the water molecules (WAT). Accordingly, the total energy difference, Δe, is divided into six component terms as the combination of two components of redox sites (HEME or SP) and the three components of the environment (CYT, RC, or WAT).

The variance−covariance matrix for the components of the total energy difference was determined using eq 11. The results are shown in Table 2. The diagonal elements are variances of corresponding terms. The upper off-diagonal terms are the covariances of two corresponding terms, and the lower off-diagonal terms (shown in italics) are the correlation coefficients between the two terms. The components of the matrix are sorted by the strength of the diagonal terms. The last row of the Table is the sum of each column of the variance−covariance matrix, which corresponds to the reorganization energy decomposition using the LRA definition (eq 12). Figure 4 shows a graphic summary of these results.

From these results, it is observed that the water and protein contributions are comparable. Although the solvent is far from the redox sites, its large contribution to the reorganization energy is a consequence of the high polarizability of the water molecules. Since the protein interior is mostly a hydrophobic environment, the contribution to the total reorganization energy becomes smaller compared to the case in which the redox sites

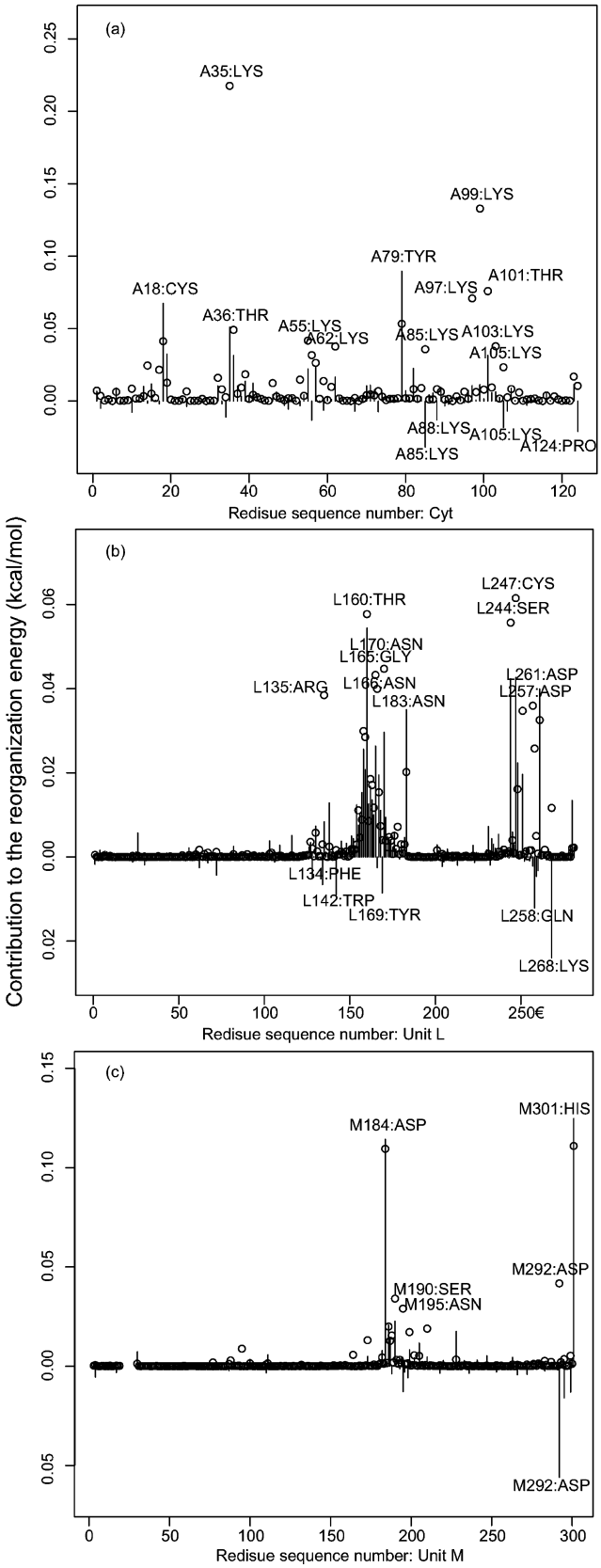

Figure 5. Contribution to the total reorganization energy from residue components (a) of cytochrome c_2 (denoted by A), (b) of the L unit of the reaction center, and (c) of the M unit of the reaction center. The diagonal term is represented by circle for each residue, and the sum (i.e., LRA definition) is represented by a line.

are surrounded by water molecules. The contributions to the total reorganization energy using the LRA definition are always

TABLE 2: Variance−Covariance Matrix Representation of the Reorganization Energy[a]

	HEME.WAT	SP.RC	HEME.CYT	SP.WAT	HEME.RC	SP.CYT
HEME.WAT	1.52	−0.05	−0.42	−0.45	−0.12	0.10
SP.RC	*−0.04*	1.39	0.35	−0.11	−0.43	−0.19
HEME.CYT	*−0.33*	*0.28*	1.09	0.06	−0.23	−0.25
SP.WAT	*−0.39*	*−0.10*	*0.06*	0.90	0.11	−0.09
HEME.RC	*−0.13*	*−0.50*	*−0.30*	*0.16*	0.55	0.07
SP.CYT	*0.16*	*−0.32*	*−0.47*	*−0.18*	*0.20*	0.26
SUM	0.58	0.95	0.60	0.42	−0.04	−0.10

[a] The total reorganization energy is decomposed in the level of a molecular unit. The upper rows are the matrix definition, eq 11. The diagonal terms represent the variance of each component in terms of the total energy difference, Δe; for example, HEME.WAT represents the component of energy difference that comes from the interaction between the heme moiety and water molecules. The upper off-diagonal terms are the covariance between terms. The lower off-diagonal terms written in italic are the correlation coefficients. The sum of the row of the variance covariance matrix is shown in the last row (labeled SUM), which corresponds to the components of the reorganization energy by the LRA definition, eq 12. All units are kcal/mol. Larger diagonal terms from the water-related term such as HEME.WAT indicate that a large part of the reorganization energy comes from the fluctuation of water molecules.

smaller than the diagonal terms of corresponding component elements since most of the covariance terms are negative. Because there are strong correlations, the partition of the reorganization energy utilizing any of the two definitions should always be used with care. In the LRA approach, the reorganization energy is divided into a set of contributions associated with different physical regions, but these contributions are not independent.

Contributions from Each Residue to the Total Reorganization Energy. The partition described above can be refined in a more detailed way to extract the interaction of individual residues with the donor and acceptor redox sites. Since a full variance−covariance matrix representation is too large at such a detailed resolution, we limit the discussion to the diagonal terms and the LRA components. Figure 5 shows the contributions for the residues of (a) the cyt c_2, (b) the unit L of RC, and (c) the unit M of RC. The diagonal terms of the variance−covariance matrix are represented by a circle, and the LRA components, by a bar.

The results show large contributions from charged residues such as Lys and Asp, and they are located on the surface region between cyt and RC. A loop around L160 shows broad contributions due to conformational fluctuation. Three residues from the M unit contribute specifically. The large difference between the diagonal term and the sum of M292 indicates the strong negative correlation of M292 to other residues.

The results show the strong contributions from charged residues such as Lys and Asp. Some polar residues such as Thr and Tyr also have strong contributions. There are numerous Lys residues surrounding the cyt c_2, and many acidic residues reside on the periplasmic surface of the RC. These electrostatic interactions have been shown to be important for the association mechanism of cyt c_2 and the RC.[52,80] Residues such as the Lys35, Lys 97, Lys99, and Thr101 of cyt c_2, which are all located in the interface region and are therefore important for the association process, also make a large contribution to the classical reorganization energy.

In cyt c_2, the contributions are mainly from the Lys residues located on the surface (protein−protein interface), which is more flexible, and not from heme ligand residues. Contributions to the classical reorganization energy from unit L are less specific than those from other parts of the system. Residues in the loop

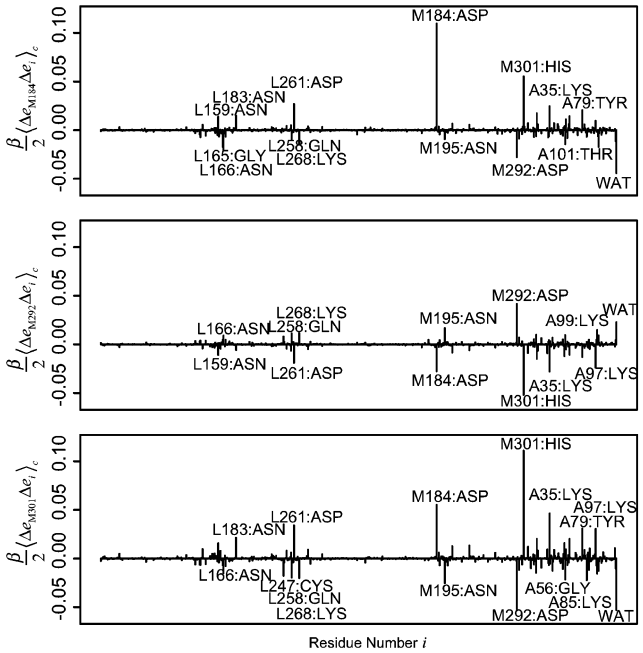

Figure 6. Correlations between residues M184 (top), M292 (middle), and M301 (bottom) and other residues. The correlation with Δe from water molecules is included at the end. The results show strong positive correlations between M184 and M301. On the contrary, M292 is negatively correlated to two other residues. These correlations should be understood carefully with the matrix representation of the total reorganization energy.

around L160 and L170 are important, especially polar residues. In addition, polar and charged residues in another loop around L250 show strong contributions. Similarly to surface residues, conformational fluctuations of these loops facilitate their participation in the reorganization energy. The influence of unit M, however, is restricted to a few very specific residues. The three residues AspM184, AspM292, and HisM301 show dominant contributions to the total reorganization energy. The C-terminal residue HisM301, which is treated as a charged C-terminal species ($-COO^-$) in our simulation, behaves like an acidic residue. The three residues are located at the surface of the RC and thus have substantial conformational flexibility. Residue M184, which has been shown experimentally to be an important residue for the binding free energy,[52] also appears to be important for the reorganization energy.

Figure 6 shows the variance−covariance elements between M184, M292, or M301 with other residues. Covariances between each of these residues and the water are also included in the plot. Note that, from the definition, the diagonal term of the variance−covariance matrix is positive. Their polarization effects are strongly correlated. M184 and M301 have positive covariances, and both are negatively correlated with AspM292. These results indicate that their motions are polarizations and are not dynamically independent. Especially, the covariance between M292 and M301 has an absolute value that is larger than the variance of M292 itself. We should emphasize, however, that although the variance−covariance matrix is needed to investigate the total reorganization energy fully it is not practical for such a detailed analysis at the residue level. A simpler analysis can determine the important residues only from the diagonal term or the LRA contribution. In addition, the difference between them indicates if correlations are important.

In summary, most of the residues with important contributions to the classical reorganization energy are located in the protein−protein interface region. Lys residues in cyt c_2 with large

contributions are located on the binding side of cyt c_2. The L region with a large contribution (L160−L170) is close to the center of the binding site. Interestingly, TyrL162, which is suggested to be a key residue for binding, almost does not contribute to the reorganization energy. Two Asp residues (M184 and M292) in the unit M are also located on the interface. Especially, M184 is close to the binding site and is shown to be an important residue for binding processes.[52] Possible effects of mutations on these residues are discussed in Conclusions.

4.3. Effect of Conformational Fluctuations on the Tunneling Pathways. Dominant Pathway in the X-ray Structure. One of the primary goals of these studies is to determine how the conformational fluctuation of protein atoms in the complex affects the tunneling matrix elements, in particular, at the protein−protein interface. As a reference for this analysis, we first calculated the Pathways decay for the "frozen" crystal structure of the cyt c_2/RC complex. The maximum coupling decay for this structure is approximately 6×10^{-5} along a pathway of atoms from the heme to a ring on the RC donor, $(BChl)_2$: HEME/CBC → TyrL162/CE1 → TyrL162/CZ → TyrL162/CE2 → $(BChl)_2$/CBC. There are two through-space jumps along this pathway: a 3.3-Å jump from HEME/CBC to TyrL162/CE1 and a 4.0-Å jump from TyrL162/CE2 to the special pair group D_A/CBC. Gray and collaborators[48] have shown that, for typical reorganization energies, the maximum ET rate (optimized Franck−Condon factor) in proteins is roughly $k_{ET} \approx 10^{14}$ or 10^{13} s^{-1} × (Pathways decay).[2] If we choose the larger prefactor, then this decay will provide an ET rate of approximately 0.4×10^6 s^{-1}. Although this number is in reasonable agreement with the typical experimentally measured rate of 10^6 s^{-1}, this computed value is still small since the measured optimized Franck−Condon rate for this reaction appears to be around 10^7 s^{-1}. (This is the maximal experimental rate when the data is analyzed assuming the Franck−Condon factor has contributions of classical and quantum modes as discussed in section 4.1. The maximum rate would be different if a simple classical mode was used in the data analysis.[32]) In addition, the Pathways calculation utilized the most favorable choice of initial and final atoms connecting donors and acceptors. They utilized the edge of the cofactors when determining the pathways. A more conservative approach would instead utilize the conjugation edge of these cofactors,[48] and the Pathways decay would be 0.36 times smaller, slowing down the rate by almost a factor of 10. These numbers, however, are still qualitative. Since the physical pathway includes two through-space jumps whose coupling may be strongly dependent on orbital overlap, more detailed quantitative analysis will soon be possible by utilizing better Hamiltonians[34] where these concerns can be quantitatively analyzed. Despite this limitation in quantitatively determining absolute rates, Pathways is sufficiently good to determine the physical nature of the pathways and how they are affected by thermal fluctuations as presented in the discussion that follows.

Structural Variation of the Tunneling Matrix Element. Figure 7a shows the variation in the electronic coupling, T_{DA}, observed during the 1-ns trajectory of the molecular dynamics simulation. From this simulation, 1000 structures were extracted at 1-ps intervals. The dominant pathway of each of these structures was then determined, and their decay was plotted in this Figure. A circle around the dots is added for those 54 structures with pathways that include water molecules.

Figure 8 shows how the magnitude of the pathways decay varies over these 1000 structures. The average value for this decay is 2.1×10^{-5}. We have calculated a decay of 5.7×10^{-5} for the X-ray structure, which is 2.7 times larger than this average value. This indicates that this crystal structure, as expected, is better packed than most of the configurations observed during the simulation. These decays vary about 10 fold, from 1×10^{-4} to 4×10^{-6}.

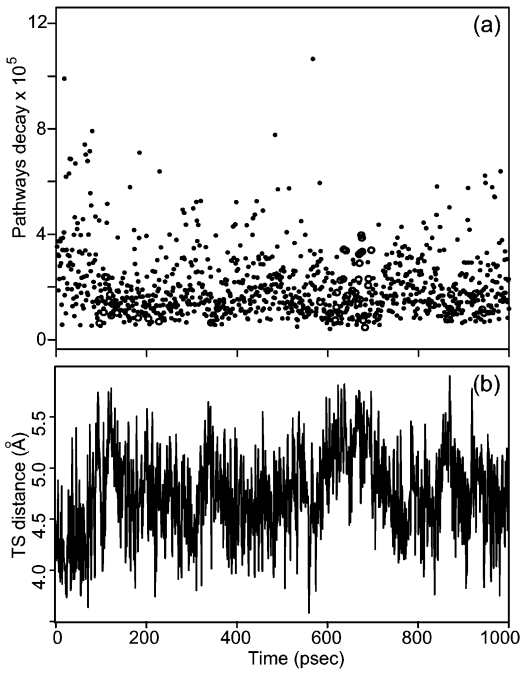

Figure 7. (a) Values for the dominant Pathways decays for structures sampled during 1-ns molecular dynamics runs. Structures were recorded every picosecond. For those structures that have a dominant pathway and include one water molecule, circles instead of dots were used to plot their decays. (b) Trajectory of the distance of through-space between HEME/CBC and TyrL162/CD1.

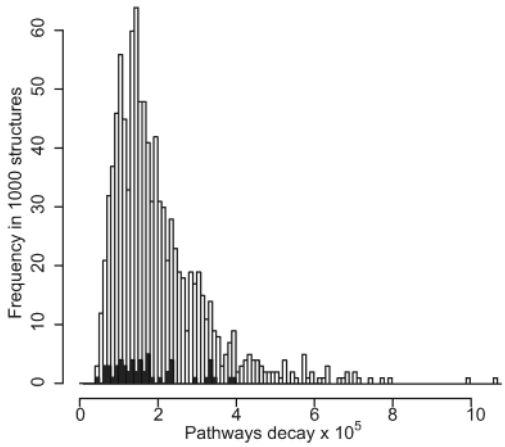

Figure 8. Distribution of the Pathways decays for the 1000 sample structures. The width of the bins is 1×10^{-6}. Black regions of histograms indicate the occurrence of dominant pathways that include water molecules. The three largest Pathways decays are 1.07×10^{-4}, 9.90×10^{-5}, and 7.91×10^{-5}. The three smallest ones are 4.07×10^{-6}, 4.62×10^{-6}, and 4.94×10^{-6}. The largest decays for dominant pathways that include one water molecule are 3.96×10^{-5}, 3.86×10^{-5}, and 3.42×10^{-5}. The three smallest ones are 4.62×10^{-6}, 6.26×10^{-6}, and 6.42×10^{-6}.

Figure 9a shows the dominant pathway observed during the entire run. This pathway is superimposed on the X-ray structure to facilitate visualization. Most of the dominant pathways for the different structures go through TyrL162, which is suggested to be the bridge for ET between cyt c_2 and the RC.[53] The through-space jump between the TyrL162/CD1 and the HEME/

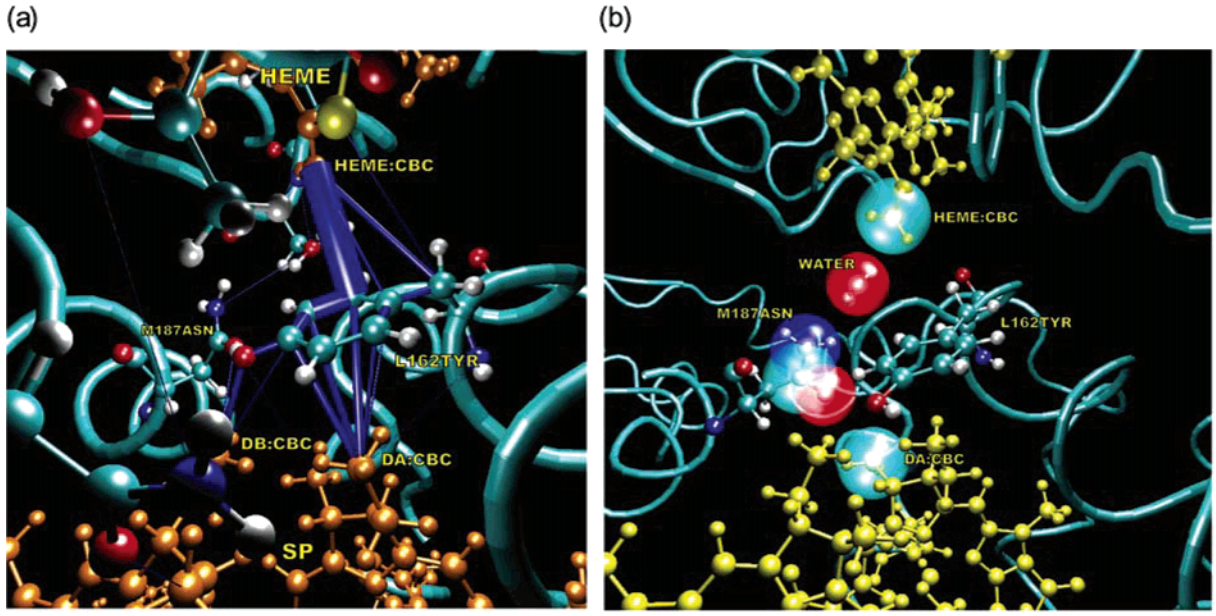

Figure 9. (a) Dominant pathways sampled during the 1-ns run superimposed on the X-ray structure. Blue lines connecting atoms represent covalent bonds; through-space jumps or hydrogen bonds involved the pathway. The thickness of the blue lines is proportional to the frequency with which each connection is included in the dominant pathways. Pathway connections that occur fewer than 10 times in the 1000 structures sampled are omitted. (b) Typical dominant pathway that includes one water molecule. Atoms included in the pathway are represented as large spheres. TyrL162 is shown, but it is not part of this dominant pathway. These images were made from VMD.[81]

CBC groups appears in most of these pathways (i.e., it can be found in the dominant path of 681 structures of the 1000 that were sampled). Thus, the through-space distance between these two atoms is an important factor in determining the strength of T_{DA}. Figure 7b shows the length fluctuation of this jump during the entire trajectory. By comparing Figure 7a and b, a clear correlation between the pathway strength and the jump distance is observed. HEME/CBC has also an important role. More than 900 dominant pathways include a through-space jump between the HEME/CBC group and one of the atoms in TyrL162. This jump between TyrL162/CD1 and HEME/CBC appears in the path of 700 structures. Regarding the special pair, 733 dominant pathways are connected to group CBC of D_A, and 127 dominant pathways are connected to group CBC of D_B.

The largest observed value for the Pathways decay is 1.07×10^{-4}. Atoms included in this pathway are HEME/CBC → TyrL162/CD1 → TyrL162/CG → TyrL162/CD2 → D_A/CBC. This large coupling is a consequence of thermal fluctuations that squeeze the through-space jumps. No special contact of atoms is needed to make the matrix element especially large. The distance between the HEME/CBC group and TyrL162/CD1 is 3.58 Å, and the distance between TyrL162/CD2 and the D_A/CBC group is 3.39 Å; these distances are smaller than the typical ones.

The atoms included in the dominant pathway for the crystal structure are common participants in most of the dominant pathways observed for the others structures that we have analyzed. This result indicates that tunneling matrix elements obtained from calculations utilizing the crystal structure can provide qualitative information about the tunneling pathway, but conformational fluctuations have to be incorporated for a quantitative determination of its strength. During our sampling run, the Pathways decay fluctuates about 10 fold (i.e., one 100-fold in the rate. Most of these fluctuations are a consequence of conformational rearrangements of TyrL162. The average decay is about three times smaller than the X-ray structure decay. This indicates that this crystal structure is better packed than most of the ones observed in our simulation. Still, thermal fluctuations can lead to even smaller decays.

Water Molecules Involved in the Pathway. Water molecules are occasionally included in the dominant pathways (i.e., in about 5% of the sampled structures). The dominant pathway for these 54 structures contains one water molecule, which includes hydrogen bonds from/to the water oxygen. The largest Pathways decay observed for these structures is 4.0×10^{-5}. A typical pathway with one water molecule, which has a decay of 2.9×10^{-5}, is shown in Figure 9b: HEME/CBC → O of a water molecule → AsnM187/ND2 → AsnM187/CG → AsnM187/OD1 → D_A/CMC. The interaction between the water and the Asn is a hydrogen bond. Most of these pathways go through AsnM187. The best pathway without going through the water for this structure has a decay of 1.12×10^{-5} ($\sim 1/3$ of the dominant one). In this structure, the through-space jumps to/from Tyr are longer than usual (e.g., the distance between the TyrL162/CD1 and the HEME/CBC of this structure is 5.5 Å). The atoms included in this pathway are uncommon (i.e., HEME/CBC → TyrL162/O → TyrL162/C → TyrL162/CA → TyrL162/N → D_A/CBC). In addition, the through-space jump between the HEME/CBC and the TyrL162/O is 3.80 Å, and the one between the TyrL162/N and the D_A/CBC is 4.20 Å. Therefore, this minor structural disorder makes the dominant pathway tube go through a water molecule instead of TyrL162.

5. Conclusions

These studies consist of the first detailed quantitative analysis of how the protein environment and its dynamical fluctuations control the interprotein ET rate in a protein complex. We are now in a position to establish a comparison with experimental data that have investigated the rate dependence of the protein−protein interface by site-directed mutagenesis. Tetreault et al.[52] have studied the electrostatic interactions governing binding and the ET reaction between cyt c_2 and the RC from *Rb. sphaeroides* by changing the charges of residues on the RC surface. These results revealed the major impact of the charged residues at the

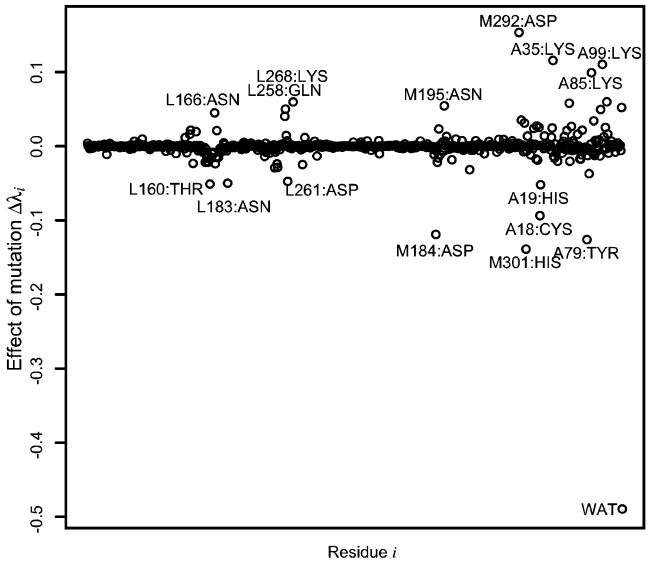

Figure 10. Shift of the total reorganization energy due to the mutation of a residue into a neutral under the assumption that the dynamics of the system is not affected by mutation. Effects due to the neutralization of the whole water molecules are included.

RC surface region in binding (residue M184, for example). The first-order ET rate constant, which is analyzed in this paper, does not change significantly. This is in total agreement with what we have observed in our calculations where we have focused on the role of the conformational fluctuation of the protein and solvent molecules in the reaction mechanism. Although the charge residues at the surface are important for the classical reorganization energy, no single one is dominant. Therefore, the impact of single mutations always has a limited effect on the total reorganization energy, as discussed in the paragraph that follows. In addition, the charged residues mutated in that study are not important to the tunneling pathway through Tyr L162, and thus their mutation would not change the rate of electron transfer if the structure of the tunneling region was unchanged. Our calculation of the classical reorganization energy leads to a result that is in agreement with the one observed experimentally, which makes us confident that our method is appropriate for the analysis performed.

Our calculations show the minor importance of specific interface residues to the total classical reorganization energy. Since our simulation was performed only for the wild-type protein, we had to determine the effect of mutations indirectly. For example, theoretically we can determine the effect of mutating the residual charges of a residue to zero.[22,82] If the partial charges of a residue *i* are modified to neutral ones and assuming that the dynamics of the remaining residues are weakly affected (a reasonable approximation), then the total classical reorganization energy would change by $\Delta\lambda_i = 2\lambda_i - \lambda_{ii}$ (i.e., the sum of the elements of a matrix representation that come from component element Δe_i values; see eqs 11 and 12). Figure 10 shows the effect of neutralizing mutations for all residues. The neutralization of whole water molecules is also evaluated. The effects of single mutations are as large as 0.15 kcal/mol, which is small compared to the total classical reorganization energy of 2.4 kcal/mol.

For electron transfer through a fixed distance, the ET rate is weakly dependent on the mutations of residues in the intervening media, thus we expect that they have a minor effect on the tunneling matrix element. Ortega et al.[53] studied the ET reaction between the tetraheme cyt *c* and the special pair of bacteriochlorophylls in the reaction centers isolated from seven strains of the photosynthetic purple bacterium *Rhodopseudomonas viridis*, in which the cytochrome is permanently bound in a fixed position. Mutations of the residue L162, located between the proximal heme c-559 and the special pair (Y (wild type) by F, W, G, M, T, or L) have almost no effect on the ET rate. For example, the rate for the mutation GlyL162 is only 5% slower than that for the wild-type TyrL162. These results are generally in accord with the pathway model in which the aromatic character of TyrL162 plays no role and the rate is only weakly dependent on the number of covalent bonds in the pathway as long as the number of through-space jumps remains constant. The unchanged rates may be due to the presence of water molecules replacing the mutated TyrL162 in the void. However, more detailed calculations must be made to understand the details of the rates. Thus, from our results, we expect that mutations on the surface of the protein would have a small effect on the tunneling matrix element as long as the overall complex structure is not changed. In contrast, mutations of residues near the tunneling interface on *Rb. sphaeroides* RCs can have large effects on the electron transfer rate because of changes in the structure of the cyt RC complex. Mutations of Tyr L162 to Ser or Gly[83,84] and those of the neighboring residue Leu M191 to Ala or Ser (Gong, X. M., unpublished work) in *Rb. sphaeroides* RCs have been found to reduce the electron-transfer rates greatly, by factors of near 100 and 10, respectively. From our results, these changes in rate are not likely due to changes in the Franck−Condon factor but to reductions in the tunneling matrix element caused by an increased distance between the cofactors due to mutation. The procedures used in this work can be used to investigate these complexes further as well as other electron-transfer complexes that are important in biological systems.

Acknowledgment. We thank Dr. H. L. Axelrod and Professor G. Feher for helpful discussions and for providing the coordinate of the co-crystal structure. Work in San Diego has been supported by the NSF (MCB-9974568 and PHY-0216576) and the NIH (GM48043). O.M. acknowledges the La Jolla Interfaces in Science (LJIS) postdoctoral training program supported by the Burroughs Wellcome Fund. Computations have been made at the UCSD Keck II computing facility (partially supported by NSF-9970199) and the San Diego Supercomputer Center.

References and Notes

(1) Axelrod, H. L.; Abresch, E. C.; Okamura, M. Y.; Yeh, A. P.; Rees, D. C.; Feher, G. *J. Mol. Biol.* **2002**, *319*, 501.
(2) Bendall, D. S. *Protein Electron Transfer*; Bios Scientific: Oxford, U. K., 1996.
(3) Cramer, W. A.; Knaff, D. B. *Energy Transduction in Biological Membranes: A Textbook of Bioenergetics*; Springer-Verlag: New York, 1990.
(4) *Electron Transfer—From Isolated Molecules To Biomolecules*; Jortner, J., Bixon, M., Eds.; Advances in Chemical Physics; Wiley: New York, 1999. Vol. 106−107.
(5) Warshel, A.; Parson, W. W. *Q. Rev. Biophys.* **2001**, *34*, 563.
(6) Feher, G.; Allen, J. P.; Okamura, M. Y.; Rees, D. C. *Nature (London)* **1989**, *339*, 111.
(7) Deisenhofer, J.; Epp, O.; Sinning, I.; Michel, H. *J. Mol. Biol.* **1995**, *246*, 429.
(8) Marcus, R. A.; Sutin, N. *Biochim.Biophys. Acta* **1985**, *811*, 265.
(9) Hopfield, J. J. *Proc. Natl. Acad. Sci. U.S.A.* **1974**, *71*, 4135.
(10) Jortner, J. *J. Chem. Phys.* **1976**, *64*, 4860.
(11) Allen, J. P.; Williams, J. C.; Graige, M. S.; Paddock, M. L.; Labahn, A.; Feher, G.; Okamura, M. Y. *Photosynth. Res.* **1998**, *55*, 227.
(12) Lin, X.; Murchison, H. A.; Nagarajan, V.; Parson, W. W.; Allen, J. P.; Williams, J. C. *Proc. Natl. Acad. Sci. U.S.A.* **1994**, *91*, 10265.
(13) Ortega, J. M.; Mathis, P.; Williams, J. C.; Allen, J. P. *Biochemistry* **1996**, *35*, 3354.
(14) Onuchic, J. N.; Blake, I. O. *An. Acad. Bras. Cienc.* **1982**, *54*, 479.

(15) Garg, A.; Onuchic, J. N.; Ambegaokar, V. *J. Chem. Phys.* **1985**, *83*, 4491.
(16) Onuchic, J. N. *J. Chem. Phys.* **1987**, *86*, 3925.
(17) Onuchic, J. N.; Wolynes, P. G. *J. Phys. Chem.* **1988**, *92*, 6495.
(18) Warshel, A.; Hwang, J. K. *J. Chem. Phys.* **1986**, *84*, 4938.
(19) Warshel, A.; Chu, Z. T.; Parson, W. W. *Science (Washington, D.C.)* **1989**, *246*, 112.
(20) Treutlein, H.; Schulten, K.; Brunger, A. T.; Karplus, M.; Deisenhofer, J.; Michel, H. *Proc. Natl. Acad. Sci. U.S.A.* **1992**, *89*, 75.
(21) Gunner, M. R.; Robertson, D. E.; Dutton, P. L. *J. Phys. Chem.* **1986**, *90*, 3783.
(22) Muegge, I.; Qi, P. X.; Wand, A. J.; Chu, Z. T.; Warshel, A. *J. Phys. Chem. B* **1997**, *101*, 825.
(23) Basu, G.; Kitao, A.; Kuki, A.; Go, N. *J. Phys. Chem. B* **1998**, *102*, 2076.
(24) Basu, G.; Kitao, A.; Kuki, A.; Go, N. *J. Phys. Chem. B* **1998**, *102*, 2085.
(25) Miyashita, O.; Go, N. *J. Phys. Chem. B* **2000**, *104*, 7516.
(26) Simonson, T. *Proc. Natl. Acad. Sci. U.S.A.* **2002**, *99*, 6544.
(27) Simonson, T.; Perahia, D. *J. Am. Chem. Soc.* **1995**, *117*, 7987.
(28) Archontis, G.; Simonson, T. *J. Am. Chem. Soc.* **2001**, *123*, 11047.
(29) Simonson, T.; Archontis, G.; Karplus, M. *J. Phys. Chem. B* **1999**, *103*, 6142.
(30) Sharp, K. A. *Biophys. J.* **1998**, *74*, 1241.
(31) Parson, W. W.; Chu, Z. T.; Warshel, A. *Biophys. J.* **1998**, *74*, 182.
(32) Venturoli, G.; Drepper, F.; Williams, J. C.; Allen, J. P.; Lin, X.; Mathis, P. *Biophys. J.* **1998**, *74*, 3226.
(33) Aquino, A. J. A.; Beroza, P.; Reagan, J.; Onuchic, J. N. *Chem. Phys. Lett.* **1997**, *275*, 181.
(34) Balabin, I. A.; Onuchic, J. N. *Science (Washington, D.C.)* **2000**, *290*, 114.
(35) Beratan, D. N.; Betts, J. N.; Onuchic, J. N. *Science (Washington, D.C.)* **1991**, *252*, 1285.
(36) Onuchic, J. N.; Beratan, D. N.; Winkler, J. R.; Gray, H. B. *Annu. Rev. Biophys. Biomol. Struct.* **1992**, *21*, 349.
(37) Page, C. C.; Moser, C. C.; Chen, X. X.; Dutton, P. L. *Nature (London)* **1999**, *402*, 47.
(38) Gehlen, J. N.; Daizadeh, I.; Stuchebrukhov, A. A.; Marcus, R. A. *Inorg. Chim. Acta* **1996**, *243*, 271.
(39) Larsson, S. *J. Am. Chem. Soc.* **1981**, *103*, 4034.
(40) Siddarth, P.; Marcus, R. A. *J. Phys. Chem.* **1993**, *97*, 2400.
(41) Balabin, I. A.; Onuchic, J. N. *J. Phys. Chem. B* **1998**, *102*, 7497.
(42) Okada, A.; Kakitani, T.; Inoue, J. *J. Phys. Chem.* **1995**, *99*, 2946.
(43) Kawatsu, T.; Kakitani, T.; Yamato, T. *J. Phys. Chem. B* **2001**, *105*, 4424.
(44) Broo, A.; Larsson, S. *J. Phys. Chem.* **1991**, *95*, 4925.
(45) Wolfgang, J.; Risser, S. M.; Priyadarshy, S.; Beratan, D. N. *J. Phys. Chem. B* **1997**, *101*, 2986.
(46) Kurnikov, I. V.; Beratan, D. N. *J. Chem. Phys.* **1996**, *105*, 9561.
(47) Skourtis, S. S.; Beratan, D. N. In *Biological Electron-Transfer Chains: Genetics, Composition, and Mode of Operation*; Canters, G. W., Vijgenboom, E., Eds.; NATO ASI Series C, Mathematical and Physical Sciences; Kluwer Academic Publishers: Dordrecht, The Netherlands, 1998; Vol. 512, p 9.
(48) Gray, H. B.; Winkler, J. R. *Annu. Rev. Biochem.* **1996**, *35*, 537.
(49) Winkler, J. R.; Di Bilio, A. J.; Farrow, N. A.; Richards, J. H.; Gray, H. B. *Pure Appl. Chem.* **1999**, *71*, 1753.
(50) Derege, P. J. F.; Williams, S. A.; Therien, M. J. *Science (Washington, D.C.)* **1995**, *269*, 1409.
(51) Beratan, D. N.; Onuchic, J. N.; Winkler, J. R.; Gray, H. B. *Science (Washington, D.C.)* **1992**, *258*, 1740.
(52) Tetreault, M.; Rongey, S. H.; Feher, G.; Okamura, M. Y. *Biochemistry* **2001**, *40*, 8452.
(53) Ortega, J. M.; Dohse, B.; Oesterhelt, D.; Mathis, P. *Biophys. J.* **1998**, *74*, 1135.
(54) Warshel, A. *J. Phys. Chem.* **1982**, *86*, 2218.
(55) Hwang, J. K.; Warshel, A. *J. Am. Chem. Soc.* **1987**, *109*, 715.
(56) Tachiya, M. *J. Phys. Chem.* **1989**, *93*, 7050.
(57) Kubo, R.; Toda, M.; Hashitsume, N. *Statistical Physics II: Nonequilibrium Statistical Mechanics*, 2nd ed; Springer: Berlin, 1991.
(58) Langen, R.; Brayer, G. D.; Berghuis, A. M.; Mclendon, G.; Sherman, F.; Warshel, A. *J. Mol. Biol.* **1992**, *224*, 589.
(59) Lee, F. S.; Chu, Z. T.; Bolger, M. B.; Warshel, A. *Protein Engineering* **1992**, *5*, 215.
(60) Aqvist, J.; Medina, C.; Samuelsson, J. E. *Protein Eng.* **1994**, *7*, 385.
(61) Archontis, G.; Karplus, M. *J. Chem. Phys.* **1996**, *105*, 11246.
(62) Gao, J.; Kuczera, K.; Tidor, B.; Karplus, M. *Science (Washington, D.C.)* **1989**, *244*, 1069.
(63) Boresch, S.; Karplus, M. *J. Mol. Biol.* **1995**, *254*, 801.
(64) Beratan, D. N.; Onuchic, J. N.; Hopfield, J. J. *J. Chem. Phys.* **1987**, *86*, 4488.
(65) Beratan, D. N.; Onuchic, J. N. *Photosynth. Res.* **1989**, *22*, 173.
(66) Onuchic, J. N.; Beratan, D. N. *J. Chem. Phys.* **1990**, *92*, 722.
(67) Beratan, D. N.; Onuchic, J. N.; Betts, J. N.; Bowler, B. E.; Gray, H. B. *J. Am. Chem. Soc.* **1990**, *112*, 7915.
(68) Regan, J. J.; Dibilio, A. J.; Langen, R.; Skov, L. K.; Winkler, J. R.; Gray, H. B.; Onuchic, J. N. *Chem. Biol.* **1995**, *2*, 489.
(69) Axelrod, H. L.; Abresch, E. C.; Okamura, M. Y.; Feher, G.; Yeh, A. P.; Rees, D. C. *Biophys. J.* **1999**, *76*, A20.
(70) Northrup, S. H.; Pear, M. R.; Morgan, J. D.; McCammon, J. A.; Karplus, M. *J. Mol. Biol.* **1981**, *153*, 1087.
(71) Miyashita, O.; Go, N. *J. Phys. Chem. B* **1999**, *103*, 562.
(72) Kashiwagi, H.; Obara, S. *Int. J. Quantum Chem.* **1981**, *20*, 843.
(73) Schmidt, M. W.; Baldridge, K. K.; Boatz, J. A.; Elbert, S. T.; Gordon, M. S.; Jensen, J. H.; Koseki, S.; Matsunaga, N.; Nguyen, K. A.; Su, S. J.; Windus, T. L.; Dupuis, M.; Montgomery, J. A. *J. Comput. Chem.* **1993**, *14*, 1347.
(74) Cornell, W. D.; Cieplak, P.; Bayly, C. I.; Gould, I. R.; Merz, K. M.; Ferguson, D. M.; Spellmeyer, D. C.; Fox, T.; Caldwell, J. W.; Kollman, P. A. *J. Am. Chem. Soc.* **1995**, *117*, 5179.
(75) Jorgensen, W. L.; Chandrasekhar, J.; Madura, J. D.; Impey, R. W.; Klein, M. L. *J. Chem. Phys.* **1983**, *79*, 926.
(76) Kraulis, P. J. *J. Appl. Crystallogr.* **1991**, *24*, 946.
(77) Case, D. A.; Pearlman, D. A.; Caldwell, J. W.; Cheatham, T. E., III; Ross, W. S.; Simmerling, C. L.; Darden, T. A.; Merz, K. M.; Stanton, R. V.; Cheng, A. L.; Vincent, J. J.; Crowley, M.; Tsui, V.; Radmer, R. J.; Duan, Y.; Pitera, J.; Massova, I.; Seibel, G. L.; Singh, U. C.; Weiner, P. K.; Kollman, P. A. *Amber*, 6th ed.; University of California: San Francisco, CA, 1999.
(78) Betts, J. N.; Beratan, D. N.; Onuchic, J. N. *J. Am. Chem. Soc.* **1992**, *114*, 4043.
(79) Lin, X.; Williams, J. C.; Allen, J. P.; Mathis, P. *Biochemistry* **1994**, *33*, 13517.
(80) Tetreault, M.; Cusanovich, M.; Meyer, T.; Axelrod, H.; Okamura, M. Y. *Biochemistry* **2002**, *41*, 5807.
(81) Humphrey, W.; Dalke, A.; Schulten, K. *J. Mol. Graphics* **1996**, *14*, 33.
(82) Muegge, I.; Schweins, T.; Langen, R.; Warshel, A. *Structure* **1996**, *4*, 475.
(83) Farchaus, J. W.; Wachtveitl, J.; Mathis, P.; Oesterhelt, D. *Biochemistry* **1993**, *32*, 10885.
(84) Wachtveitl, J.; Farchaus, J. W.; Mathis, P.; Oesterhelt, D. *Biochemistry* **1993**, *32*, 10894.